



# Corrosion film breakdown of galvanized steel in seawater below 25 °C

Jhon E. Torres-Ramirez<sup>1</sup> · Anderson Sandoval-Amador<sup>2</sup> · Luisa Fernanda Ortiz-Vasquez<sup>2</sup> · Darío Yesid Peña-Ballesteros<sup>3</sup> · José Luis Endrino<sup>2</sup>

Received: 10 October 2023 / Accepted: 4 January 2024  
© Qatar University and Springer Nature Switzerland AG 2024

## Abstract

Galvanized steel is one of the main materials used today due to its mechanical properties and corrosion resistance; among multiple applications, it is used in the construction of metal and concrete structures. Galvanized steel is a material made of carbon steel SAE/AISI 1010 covered with a zinc surface that supplies steel with significant protection against corrosion. Although the physicochemical and electrochemical behavior of galvanized steel has been studied in multiple environments of service under different conditions; very few studies have focused on analyzing the performance of this material below room temperature (25 °C). Clearly, galvanized steel is exposed to low seawater temperatures in environments where the climate temperature is between 25 and 0 °C. This research work evaluates the electrochemical behavior of galvanized steel samples with three different coatings thicknesses (0.0043 g·cm<sup>-2</sup>, 0.0080 g·cm<sup>-2</sup>, and 0.0135 g·cm<sup>-2</sup>) using simulated seawater solution in a temperature range between 0 and 25 °C. The results obtained allow understand better the effect of temperature on the corrosion of galvanized steel exposed in environments at temperatures below 25 °C. The data obtained show that there is an inverse correlation between the thickness of the Zn coating and the corrosion rate; on the other hand, by decreasing the working temperature from 25 to 0 °C, a slight increase in the kinetics of the corrosion process was obtained, this being a result of great relevance in the industry and scientific research.

**Keywords** Galvanized steel · Corrosion · Electrochemical test · Zinc film

## 1 Introduction

Galvanized steel (GS) is a widely used material in different types of applications due to its excellent properties [1–5]. The GS is used in industries such as transportation (parts of cars, motorcycles, and airplanes such as the “body-in-white,” hoods, frames, and door fittings [6, 7]), construction (pieces such as awnings, balconies, ductwork, handrails, fences, ladders, street furniture, and support beams [8]), electronics (computers casings, precision instruments), and among other industries.

GS is a material consisting of carbon steel as a base material coated mainly with a layer of zinc (Zn) [9]; GS presents high mechanical resistance for two reasons. On the one hand, carbon steel works as a base or structural material; on the other hand, the zinc coating protects the steel with good resistance against corrosion and attrition. Zinc protects steel in three ways: It serves as a physical barrier preventing aggressive or corrosive agents from contact with steel; it also performs cathodic protection for zinc and has a more active character than steel, sacrificing itself to any metal higher (nobler) than zinc in the periodic table. When Zn reacts with different agents present in the environment, it allows the formation of different zinc compounds on the material’s surface, which gives an additional protective barrier to steel [10].

The degradation of GS is produced to a greater extent in environments with the presence of corrosive agents such as chloride or sulfate, as it is in industrial and coastal environments where the concentration of salt in the atmosphere is high; the main environment that affects the corrosion of the most of metals is when the metals are in contact with

✉ Anderson Sandoval-Amador  
aasandoval@uloyola.es

<sup>1</sup> CONICET-Comisión Nacional de Energía Atómica, Buenos Aires, Argentina

<sup>2</sup> Materials and Sustainability Group, Universidad Loyola Andalucía, Dos Hermanas, Sevilla, Spain

<sup>3</sup> Grupo de Investigaciones en Corrosión, Universidad Industrial de Santander, Bucaramanga, Colombia

**Fig. 1** Corrosion mechanism of galvanized steel; adapted of [9]

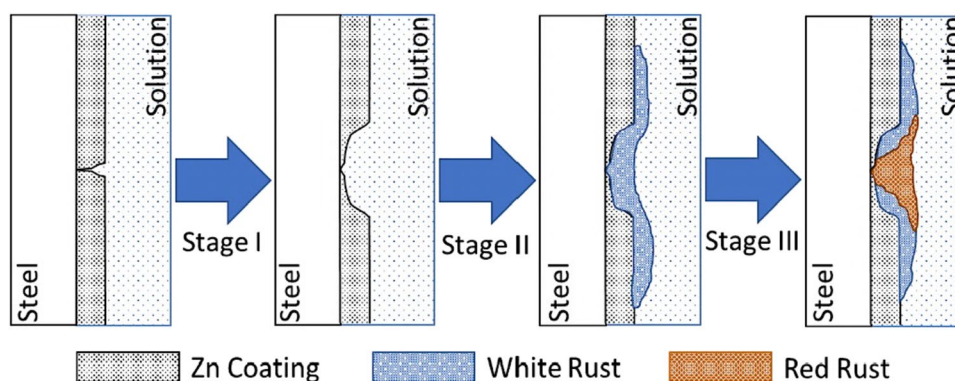


**Table 1** Chemical composition of the carbon steel

Elements	Fe	C	Si	Mn	S	Ni	Cu
Value (wt.%)	97.160	0.104	0.029	0.287	<0.150	0.316	1.050

seawater [11, 12]. The most relevant factors that make seawater a highly corrosive electrolyte are salinity, conductivity, pH of dissolved oxygen, and among other physical factors. Dissolved salts in the electrolyte (for example, NaCl) not only increase the conductivity of the electrolyte but can destroy passive films on the surface of metals by the influence of chloride ion and promote localized acidification which it could generate pitting corrosion [13].

The corrosion of GS (see Fig. 1) is given, initially, by the dissolution of the Zn coating on the surface of the material and near of the coating defects (Stage I). In this stage, the Zn coating acts as a sacrificial anode. The corrosion process is followed by the formation of some products (white rust) on its surface that causes the progressive growth of a passive barrier [14]. The white rust ( $ZnO$  and  $ZnCl_2 \cdot 4Zn(OH)_2$ ) is formed by the anodic dissolution of Zn. Finally (stage III), the steel corrosion takes place due to the formation of amount of red rust (iron oxides, e.g.,  $FeOOH$ ) on the surface as a product by the dissolution of iron through the defects coating [15].

To obtain a high corrosion-resistance GS, it is essential to control some parameters during its manufacturing process, such as the chemistry of the steel, the morphology of the base material, the chemical composition of the Zn bath which is used to form the coating, the final chemical composition, and the morphology of the coating, among others [11–15]. With an optimal coating, the corrosion of the base metal will be reduced; hence, this Zn coating will form compounds, mainly Zn oxide, generating an adherent protective layer that protects steel. Many studies have focused on the electrochemical analysis of GS in different environments at room temperature or at temperatures above 25 °C. However, little has been said about its behavior at low temperatures (between 0 and laboratory temperature) since the kinetic effect of temperature is neglected. GS can be exposed to low

**Table 2** Thickness of galvanized steel sheets

Sample	S1	S2	S3
Thickness ( $g \cdot cm^{-2}$ )	0.0043	0.0080	0.0135

temperatures for two reasons, either because the design of its application requires it or because the temperature drops in regions where the changes in seasons are considerable. For this reason, the electrochemical behavior of GS is studied with different thicknesses at temperatures between 0 and 25 °C approximately to evaluate if there is any considerable change in its performance as a passive barrier of GS in simulated coastal environments.

## 2 Methods

The experimental method in this work was sequentially developed as follows: substrate preparation, electrochemical characterization, and surface damage analysis.

### 2.1 Materials

The galvanized steel was commercially acquired. In this research work, SAE/AISI 1010 carbon steel sheets were used (2 mm of thickness), whose elemental chemical composition was obtained by means of the elemental atomic absorption analysis by arc spark (Table 1) [16]. The Zn coating was performed by means of a hot immersion process in a Zn-aluminum (Al) bath at 450 °C, approximately; the composition of the bath was 99.5% Zn and 0.5% Al approx. Galvanized steel sheets were manufactured with three different thicknesses (see Table 2). It should be noted that the thicknesses of the sheets of GS were provided by the manufacturer. For

this, the guidelines of ASTM A123/A123M-15 [17] were followed.

## 2.2 Electrochemical test

The GS sheets with the three levels of thickness were cut into  $20 \times 20$  mm specimens; all GS square samples were cleaned with acetone in an ultrasonic bath for 20 min approximately to remove any type of dirt or oil. Subsequently, the samples were dried with hot air and stored in a desiccator with a controlled atmosphere to avoid any reaction with the environment. Perforation was performed on each sample, leaving a hole of 2.0 mm in diameter to join the sheets to a copper wire, which would serve as an electrical contact for the connection with the potentiostat; each specimen was coated with epoxy resin to isolate the wire/specimen connection and to delimit an effective area of  $1.0 \text{ cm}^2$ , approximately, which is in contact with the solution. The electrolyte (solution) used to expose and to make the electrochemical tests was a

solution whose composition remained constant in all measurements, and which simulates seawater (see Table 3); the electrolyte was prepared taking into consideration the ASTM D 1141-98 standard [18].

The electrochemical behavior of galvanizing was assessed using different electrochemical techniques; all measurements were made on a Gamry Reference 600 potentiostat/galvanostat. A three-electrode electrochemical cell, with a volume of 100 ml, was used (see Fig. 2). As a working electrode (WE), a GS sample with different coating levels of thickness was used; a counter electrode (CE) high-purity graphite bar was also used; and the reference electrode (RE) was silver/silver chloride (Ag/AgCl) with 3M KCl. The RE was placed inside a Luggin capillary that contained a saturated KCl solution, allowing conductivity inside, and the Luggin had a semi-permeable porous plug at the tip separating the two solutions; the tip of the Luggin was separate from the WE by 3 mm approximately. All the potentials shown in this work were presented according to the Ag/AgCl electrode.

Electrochemical characterization of GS samples with three different thicknesses and four temperatures was carried out; the temperatures assessed were  $0^\circ\text{C}$ ,  $5^\circ\text{C}$ ,  $15^\circ\text{C}$ , and  $25^\circ\text{C}$ , with a variation of  $\pm 1^\circ\text{C}$ . Initially, in each sample, the open circuit potential (OCP) was measured for 1 h, thus allowing to reach a stable potential of the working sample. After the OCP measurement, a potentiodynamic polarization curve (PPC) was recorded from an initial potential of  $-1.5$  to  $0.8 \text{ V}_{\text{Ag/AgCl}}$ , with a sweep speed of  $0.01 \text{ V s}^{-1}$ .

The OCP-PPC sequence was performed in each GS sample with triplicate measurements for each of the thicknesses and temperatures analyzed; some tests were discarded because some surface defects were discovered that are not representative of conditions of the standard coating (e.g., coating discontinuity, voids, surface damage, and

**Table 3** Composition of sea water simulated

Component		Percentage
Sodium chloride	NaCl	58.5%
Magnesium chloride	$\text{MgCl}_2 \cdot 6\text{H}_2\text{O}$	26.5%
Sodium sulfate	$\text{Na}_2\text{SO}_4$	9.8%
Calcium chloride	$\text{CaCl}_2$	2.8%
Potassium chloride	KCl	1.6%
Sodium bicarbonate	$\text{NaHCO}_3$	0.5%
Potassium bromide	KBr	0.2%
Boric acid	$\text{H}_3\text{BO}_3$	0.07%
Strontium chloride	$\text{SrCl}_2 \cdot 6\text{H}_2\text{O}$	0.09%
Sodium fluoride	NaF	0.007%

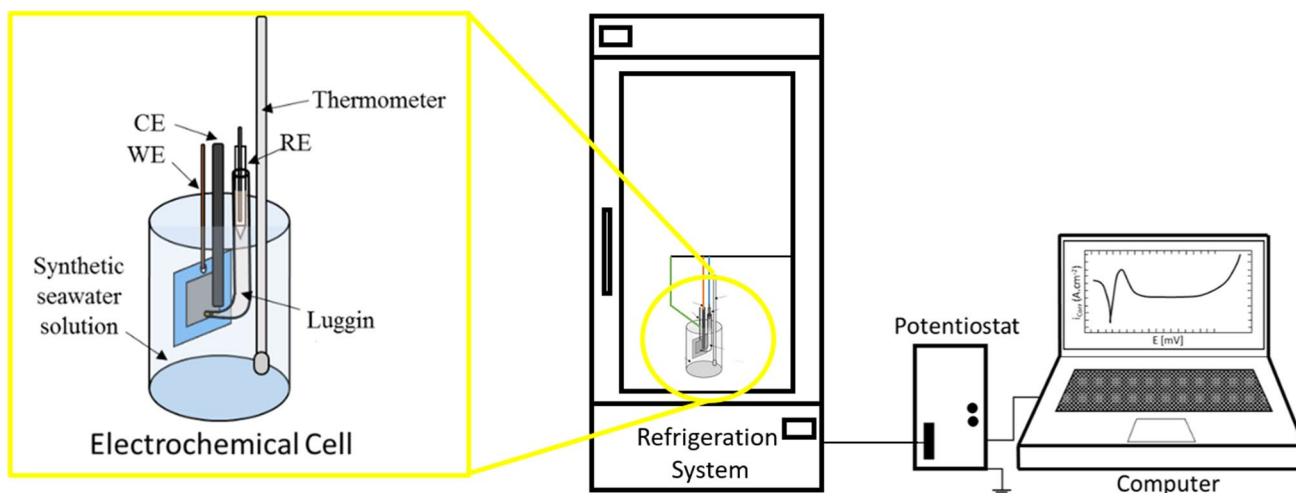


**Fig. 2** Electrochemical cell with three electrodes: work electrode (WE), counter electrode (CE), and reference electrode (RE)

loss of coating). Results shown in this article correspond to the average values of all the determined parameters, and each PPC plots show a representative curve in every single measurement.

Among the different parameters assessed, the corrosion current density ( $i_{\text{Corr}}$ ), which is directly related to the GS corrosion rate according to Faraday's law, was calculated with the Stern-Geray equation (see Eq. (1)); the polarization resistance ( $R_p$ ) values were determined in a potential of  $\pm 0.02$  V against the corrosion potential ( $E_{\text{Corr}}$ ) and the Stern-Geray constants of proportionality ( $B$ ) from anodic and cathodic Tafel slope in each curve PPC [19].

$$i_{\text{Corr}} = \frac{B}{R_p} \quad (1)$$

### 2.3 Surface damage characterization

After electrochemical tests, representative samples of each condition were selected to assess the surface damage on the GS specimens by scanning electron microscopy (SEM). The electron microscope used was a Carl Zeiss EVO MA90 scanning electron microscope which incorporated an energy dispersive X-ray spectroscopy detector.

## 3 Results and discussions

Relevant parameters can be established in the PPCs; these parameters allow to assess the kinetics of the corrosion and dissolution process of the GS [20, 21]. In Fig. 3, it is possible to see the PPCs measured in the GS for the three thicknesses studied at all exposure temperatures. In general terms, the trends of all curves are very similar;  $E_{\text{Corr}}$  values do not present significant variation with the change of temperature, since only a deviation of 15 mV was calculated (see Table 4). In addition, the PPCs show that from  $E_{\text{Corr}}$  there is an increase of the current density in the anodic sense up to potential values of  $-0.380$  V<sub>Ag/AgCl</sub> approximately, reaching values of the order of  $5 \times 10^{-2}$  A.cm<sup>-2</sup>, where the GS has a passive behavior or passivation potential ( $E_{\text{Pa}}$ ). In terms of  $E_{\text{Pa}}$  values, the current density is the passivation current density ( $i_{\text{Pa}}$ ); from  $E_{\text{Pa}}$ , the current density was stabilized, and it showed a standard passive region, where there is little variation of the current during the potential sweep process [22]. At potentials of about  $-0.2$  V<sub>Ag/AgCl</sub>, approximately, there is a small decrease in current in a short range of potential in all cases. Subsequently, the current density values are restored to similar values before the inflection point, increasing slightly until the end of the potential sweep.

**Fig. 3** CPP measured in the thickness: **a** S1, **b** S2, and **c** S3, at temperatures of 0 °C, 5 °C, 15 °C, and 25 °C

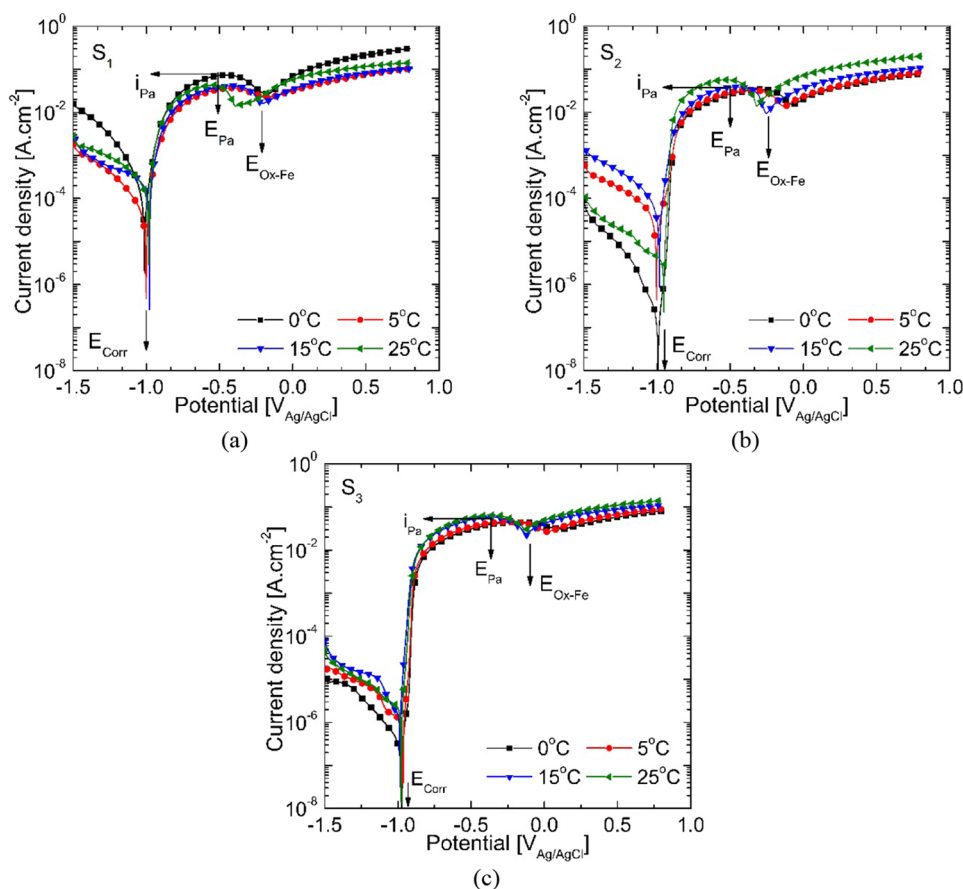
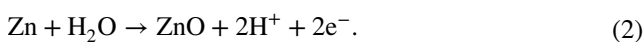


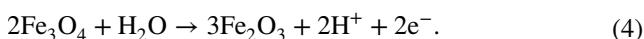
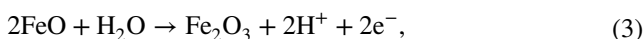
**Table 4** Average values of  $E_{\text{Corr}}$ ,  $i_{\text{Corr}}$ ,  $E_{\text{Pa}}$ ,  $i_{\text{Pa}}$ , and iron oxidation potentials ( $E_{\text{Ox-Fe}}$ ) in all temperatures assessed

Sample	$T$ (°C)	$E_{\text{Corr}}$ (V <sub>Ag/AgCl</sub> )	$i_{\text{Corr}}$ (A.cm <sup>-2</sup> )	$E_{\text{Pa}}$ (V <sub>Ag/AgCl</sub> )	$i_{\text{Pa}}$ (A.cm <sup>-2</sup> )	$E_{\text{Ox-Fe}}$ (V <sub>Ag/AgCl</sub> )
S <sub>1</sub>	0	-1.012 ± 0.04	7.28 ± 0.21 × 10 <sup>-5</sup>	-0.464 ± 0.01	7.33 ± 0.02 × 10 <sup>-2</sup>	-0.178 ± 0.19
	5	-1.001 ± 0.08	2.59 ± 6.1 × 10 <sup>-5</sup>	-0.407 ± 0.03	3.71 ± 0.01 × 10 <sup>-2</sup>	-0.171 ± 0.03
	15	-0.982 ± 0.08	1.08 ± 2.3 × 10 <sup>-4</sup>	-0.416 ± 0.03	4.14 ± 0.01 × 10 <sup>-2</sup>	-0.205 ± 0.01
	25	-0.984 ± 0.05	1.02 ± 1.1 × 10 <sup>-4</sup>	-0.543 ± 0.04	4.36 ± 0.15 × 10 <sup>-2</sup>	-0.397 ± 0.03
S <sub>2</sub>	0	-0.993 ± 0.07	1.88 ± 3.0 × 10 <sup>-7</sup>	-0.300 ± 0.01	3.35 ± 0.01 × 10 <sup>-2</sup>	-0.073 ± 0.02
	5	-1.003 ± 0.03	2.13 ± 1.8 × 10 <sup>-5</sup>	-0.351 ± 0.02	3.29 ± 0.01 × 10 <sup>-2</sup>	-0.132 ± 0.01
	15	-0.984 ± 0.07	3.26 ± 1.9 × 10 <sup>-5</sup>	-0.463 ± 0.01	3.87 ± 0.01 × 10 <sup>-2</sup>	-0.253 ± 0.02
	25	-0.953 ± 0.04	3.46 ± 0.4 × 10 <sup>-6</sup>	-0.520 ± 0.03	5.69 ± 0.17 × 10 <sup>-2</sup>	-0.320 ± 0.38
S <sub>3</sub>	0	-0.975 ± 0.09	2.54 ± 4.0 × 10 <sup>-7</sup>	-0.179 ± 0.02	4.47 ± 0.02 × 10 <sup>-2</sup>	0.110 ± 0.15
	5	-0.966 ± 0.05	1.11 ± 0.71 × 10 <sup>-6</sup>	-0.253 ± 0.03	4.55 ± 0.05 × 10 <sup>-2</sup>	0.020 ± 0.04
	15	-0.985 ± 0.02	1.40 ± 0.42 × 10 <sup>-6</sup>	-0.354 ± 0.03	5.94 ± 0.11 × 10 <sup>-2</sup>	-0.127 ± 0.02
	25	-0.976 ± 0.04	2.00 ± 0.62 × 10 <sup>-6</sup>	-0.368 ± 0.05	6.42 ± 0.13 × 10 <sup>-2</sup>	-0.128 ± 0.03

According to the bibliography [14, 23–26], the increase of the current density between  $E_{\text{Corr}}$  and  $E_{\text{Pa}}$  corresponds to the anodic process of dissolution of the zinc coating, controlled by an activation or charge transfer process; the dissolution reaction of Zn in aqueous solutions is given by the following reaction (see Eq. (2)).



Additionally, the small decrease in density at potentials of -0.2 V, approximately, is probably due to the formation of a product that helps to temporarily protect the galvanized steel; that inflection point can be described as a potential of iron oxidation ( $E_{\text{Ox-Fe}}$ ) to produce, from the transformation of  $\text{Fe}^{+2}$  to  $\text{Fe}^{+3}$ , the compound  $\text{Fe}_2\text{O}_3$  on the surface, which reduces the active area of the GS partially protecting the sample. The average values of  $E_{\text{Ox-Fe}}$  can be seen in Table 4; according to the Pourbaix diagram of iron in water at 25 °C, the oxidation reactions are represented by Eqs. (3) and (4) [23].



From the PPCs, corrosion potentials of GS did not show great variation regarding the change in temperature (see Table 4). The potential values presented deviations with reference to the mean value of  $E_{\text{Corr}}$  of 14 mV, 22 mV, and 8 mV for the thicknesses S<sub>1</sub>, S<sub>2</sub>, and S<sub>3</sub>, respectively; this indicates that the corrosion potential is not an electrochemical parameter that shows the state of attrition of GS exposed to the conditions at stake of this research work.

Contrary to what was observed with  $E_{\text{Corr}}$ , the steel presented a greater variation in the corrosion current density (or corrosion rate of GS) in all conditions assessed. According with the  $i_{\text{Corr}}$  values for all thicknesses in the

Table 4, it is possible to see that, for thicknesses S<sub>1</sub> and S<sub>3</sub> cases, there is a slight increase in the  $i_{\text{Corr}}$  values or corrosion rate of the GS with the increase of temperature, for the kinetics of the chemical reactions involved in the corrosion process grows with temperature.

The intermediate thickness (S<sub>2</sub>) initially presented an increase of  $i_{\text{Corr}}$  with rising temperature until reaching 15 °C, where the decay of the corrosion current was subsequently evidenced. This last behavior can be explained because the current peak associated with the formation of ZnO (Eq. (2)) is the highest for that thickness at 25 °C, which indicates that more Zn was dissolved from the coating to form the oxide that protects galvanized steel to a greater extent.

To better understand the behavior of GS with reference to the corrosion rate (or  $i_{\text{Corr}}$ ), as a function of the amount of coating, the  $i_{\text{Corr}}$  values against coating thickness were plotted. In Fig. 4, an inversely proportional behavior can be seen between the thickness of the GS sheets and the  $i_{\text{Corr}}$  for each temperature.

To find a relationship between these two variables ( $i_{\text{Corr}}$  vs thicknesses), a linear adjustment was made according to Eq. (5).

$$\text{Log}(i_{\text{Corr}}) = a + b \times \text{Log}(S), \quad (5)$$

where  $i_{\text{Corr}}$  is given in A cm<sup>-2</sup> and  $S$  is the thickness of the coating. The linear fit parameters of the above equation can be seen in Table 5.

In Fig. 4, the expected results are evidenced in terms of the decrease in the corrosion rate and the increase in the thickness of the GS coating. It is also observed that at temperatures of 0 °C and 5 °C, the linear adjustment is not as good as that carried out at higher temperatures (see Table 5). This is possibly because as the temperature increases, the kinetic processes of the protective products



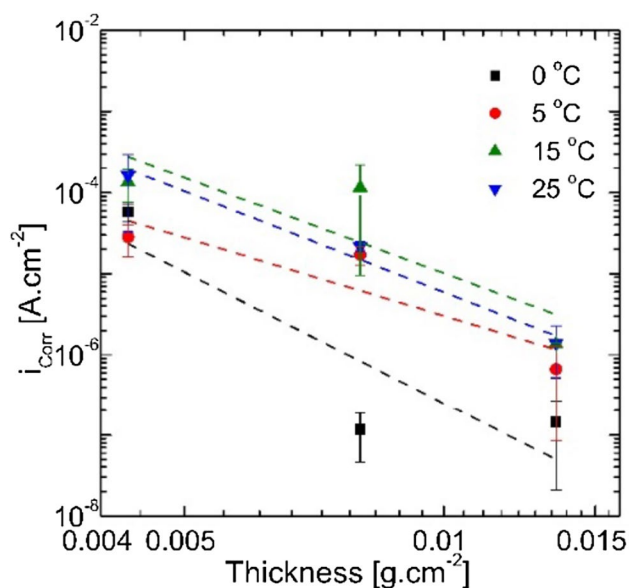


**Fig. 4** Coating thickness vs  $i_{\text{Corr}}$  density at temperatures of 0 °C, 5 °C, 15 °C, and 25 °C

**Table 5** Linear adjustment parameters between  $i_{\text{Corr}}$  and thickness for each temperature

Temperature (°C)	$A$	$b$	$R^2$
0	$-17.36 \pm 6.27$	$-5.38 \pm 2.96$	0.54
5	$-11.92 \pm 3.27$	$-3.20 \pm 1.54$	0.62
15	$-12.82 \pm 4.98$	$-3.91 \pm 2.35$	0.62
25	$-13.50 \pm 1.21$	$-4.13 \pm 0.57$	0.96

formation are favored, so that the surface of the sample present a more stable behavior against corrosion.

According to the bibliography, the formation of ZnO on the surface of the GS serves as a temporary passive barrier or layer that protects the steel [15]. The measured  $i_{\text{pa}}$  values were analyzed (directly related to the formation of ZnO); these values were of the order of  $10^{-2} \text{ A}\cdot\text{cm}^{-2}$  (see Table 5); to determine the amount of dissolved mass of zinc in the anodic polarization for the formation of ZnO, Faraday's law was used (see Eq. (6)) [25].

$$m_{\text{Zn}} = \frac{i_{\text{pa}} \cdot \text{PM}_{\text{Zn}} \cdot t}{n \cdot F} \quad (6)$$

where  $m_{\text{Zn}}$  is the dissolved mass of Zn of the coating in  $\text{g}\cdot\text{cm}^{-2} \cdot \text{s}^{-1}$ ;  $i_{\text{pa}}$  is the maximum dissolution current of the coating in  $\text{A}\cdot\text{cm}^{-2}$ ;  $\text{PM}_{\text{Zn}}$  is the molar mass of zinc ( $65.38 \text{ g}\cdot\text{mol}^{-1}$ );  $F$  is Faraday's constant ( $96,485 \text{ C}\cdot\text{mol}^{-1}$ );  $t$  is time in seconds; and  $n$  is the valence number of zinc as an ion in solution ( $n = 2$ ). Table 6 shows the values obtained from the

**Table 6** Lost mass of Zn by anodic dissolution of the coating

Temperature (°C)	Lost mass of Zn ( $M_{\text{Zn}}$ ) [ $\text{g}\cdot\text{cm}^{-2}$ ]		
	$S_1$	$S_2$	$S_3$
0	0.0014	0.0008	0.0012
5	0.0007	0.0007	0.0011
15	0.0008	0.0007	0.0013
25	0.007	0.0008	0.0013

mass of the zinc in the dissolution process when the sample was polarized;  $E_{\text{Corr}}$  to  $E_{\text{pa}}$  potentials were calculated from the  $i_{\text{pa}}$  values in each case, for 60 s, which is the approximate polarization length.

According to Table 6, Zn dissolution of the coating increases progressively with the rise of temperature, being more notable at 15 °C and 25 °C. However, a clear relationship between dissolved Zn and decrease in corrosion rate (or  $i_{\text{Corr}}$ ) is not evident, except for the data obtained in the sample with intermediate thickness ( $S_2$ ), where there is a decrease in the corrosion rate with an increase of Zn dissolution at 25 °C, probably forming ZnO that creates the passive layer on the steel. The lack of relationship between  $i_{\text{Corr}}$  and dissolution of Zn might be due to the short duration of the test and stationery, or stable conditions of the system would not be reached, so it would be expected that when running tests with slower sweep speeds, a proportional relationship between the two factors is evident.

Micrographs obtained from galvanized steel surfaces exposed to the simulated seawater solution are shown as follows. Figure 5 shows three micrographs that correspond to GS samples for the three analyzed thicknesses that were exposed to the electrolyte at different temperature, and Fig. 5d shows the linear sweep of the chemical composition of some chemical elements from the surface through the coating to the base metal. From the micrographs, it can be established that, although the coating tends to protect the steel, the quality of the samples' coating with thickness  $S_1$  (Fig. 5a) presents greater irregularity or heterogeneity. However, the micrographs of the thicknesses  $S_2$  (Fig. 5b) and  $S_3$  (Fig. 5c) show more homogeneous and therefore more protective coatings; these characteristics are corroborated in Fig. 5d. The presence of oxygen within the coating is lower in the latter coatings. Moreover, it is possible to highlight that even though the coating is more homogeneous in thicknesses  $S_2$  and  $S_3$ , the coating deposition process plays a role in its quality, since cracks could be generated in the coating, and these would affect its stability and protective quality as can be seen in the transversal section morphology of the GS samples and the chemical composition.

In Fig. 6, it can be seen the presence of precipitates of salts rich in Cl and Na formed on the surface of the steel.

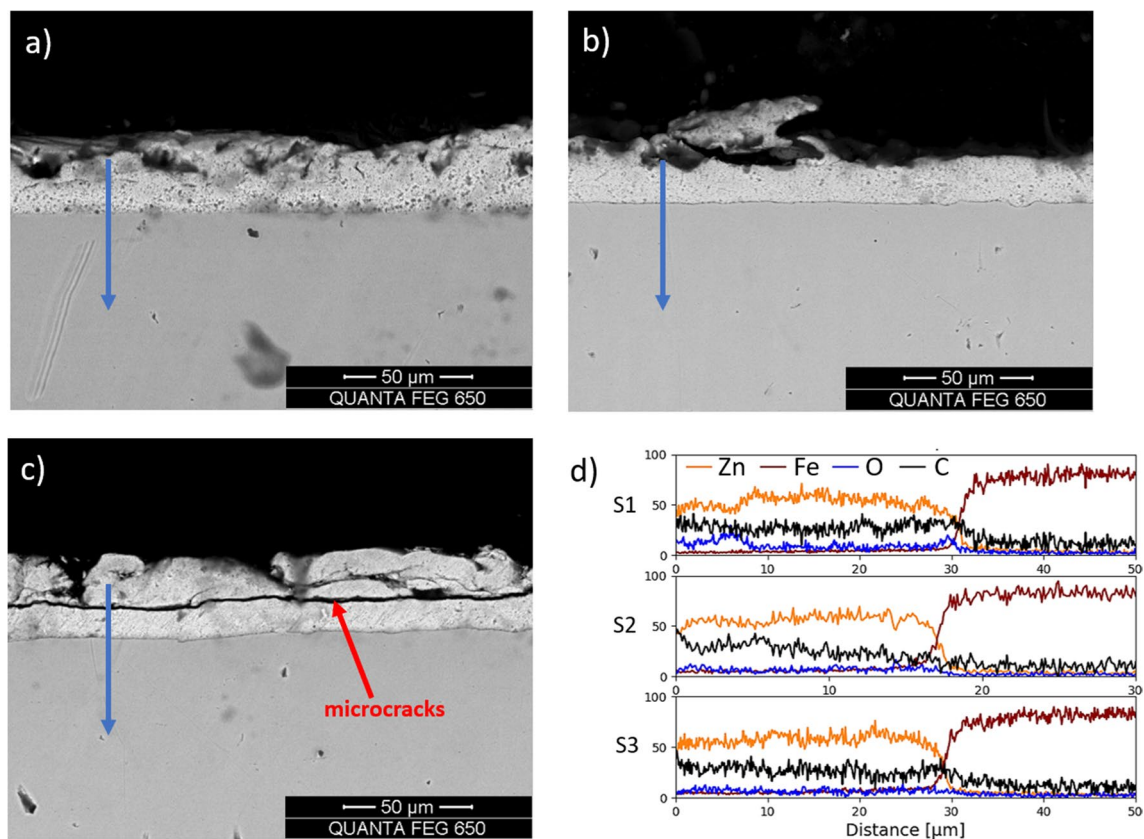


**Fig. 5** SEM micrograph for each thickness of galvanized steel: **a** S<sub>1</sub>, **b** S<sub>2</sub>, **c** S<sub>3</sub>, and **d** elemental chemical composition for a linear sweep from the sample surface to the base metal (blue arrow on micrographs)

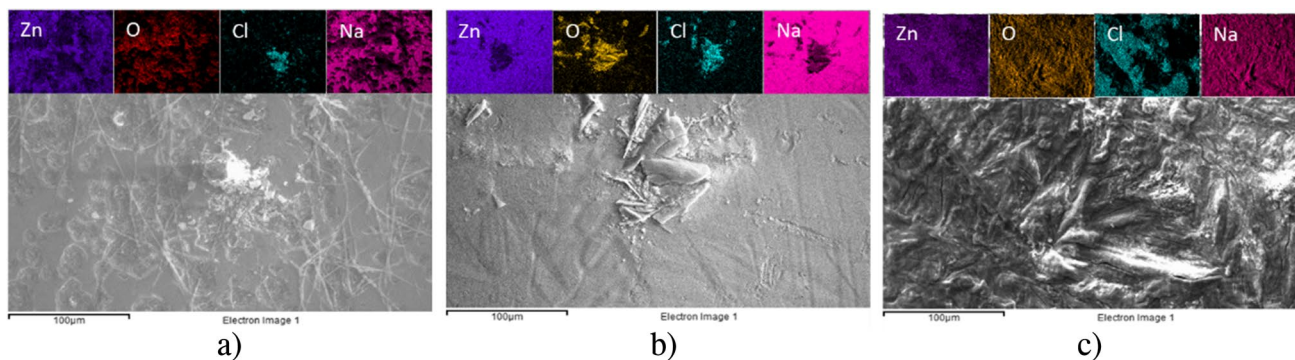


**Fig. 6** SEM-EDS surface characterization of GS after 7 days exposed at simulated sea water. **a** S<sub>1</sub>, **b** S<sub>2</sub>, and **c** S<sub>3</sub>; all micrographs show surfaces exposed at room temperature 25 °C

These elements come from the chemical components of simulated seawater. On the other hand, the surface damage presented in the steels that have smaller thicknesses (S<sub>1</sub> and S<sub>2</sub>) is less than that observed in the thicker samples (S<sub>3</sub>). This agrees with the results established in the dissolution of Zn (Table 6), since in thickness S<sub>3</sub> was where the greatest dissolution of the coating was obtained, which can eventually form Zn oxides that help protect the steel from corrosive

agents present in the working electrolyte. Furthermore, in sample S<sub>3</sub>, the elements oxygen and zinc are distributed more homogeneously on the surface of the sample, which correlates with the formation of protective ZnO on the surface of the steel, achieving a decrease in the corrosion rate of the steel (Table 4). Furthermore, in Fig. 7, it can be seen as the Zn coating thickness increases, the presence of iron oxides is lower and the distribution of these oxides is more

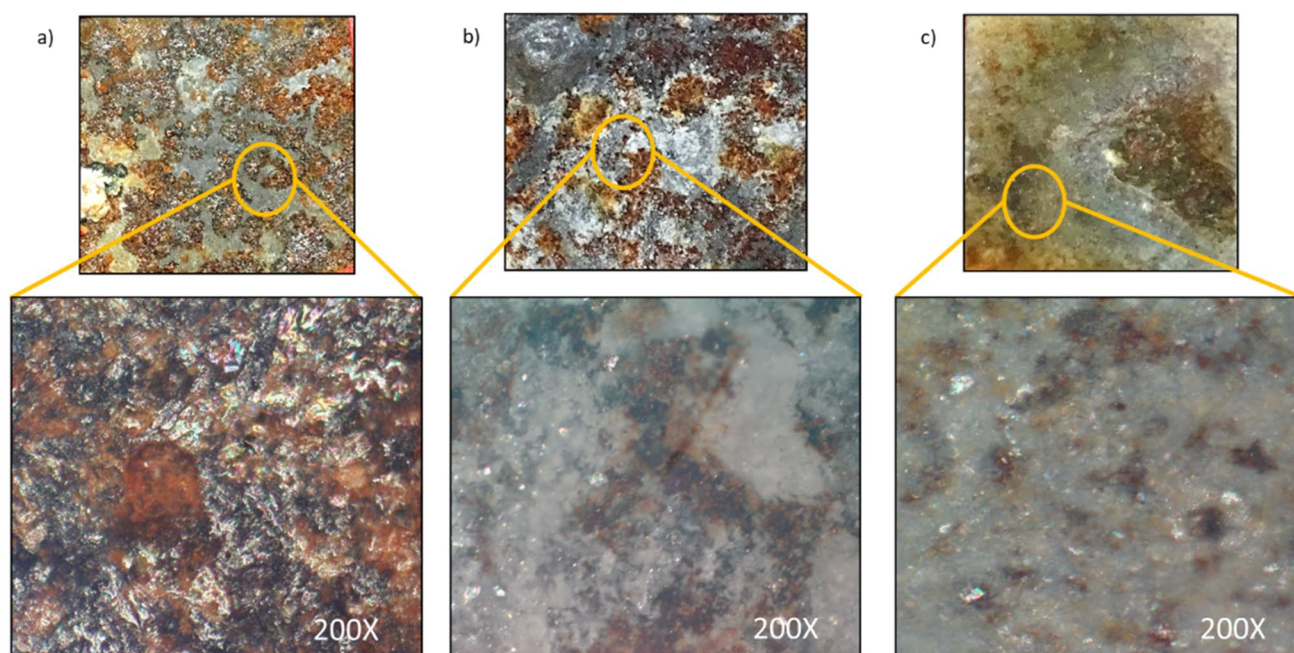


**Fig. 7** Optic micrographic surface characterization of GS after 30 days exposed at simulated sea water. **a** S1, **b** S2, and **c** S3; all micrographs show surfaces exposed at 25 °C

homogeneous; this is due to the formation of homogeneous Zn oxides (ZnO) on the surface of the steel that protects the steel from the corrosive effect of the electrolyte.

## 4 Conclusions

This research was carried out to make a contribution to the current state of knowledge on the corrosion of galvanized steel exposed to the temperatures below 25 °C. The results obtained show that at the range of studied temperatures (0 °C, 5 °C, 15 °C, and 25 °C), there was no significant variation of the  $E_{\text{Corr}}$  in the samples with different thicknesses, since there was only one variation of 16 mV observed in all cases. Therefore, this electrochemical parameter does not function as a comparison factor for the state of galvanized steel exposed to the working conditions (simulated solution of seawater at low temperatures).

In addition, experimental results revealed that the thickness of the coating plays a crucial role in mitigating the corrosion of steel in galvanized steels, since a decrease in the corrosion rate ( $i_{\text{Corr}}$ ) was observed with the increment of coating thickness. Such trend may be due to the protective function of the zinc coating. Firstly, the coating functions as a physical barrier covering the surface of the steel and minimizing its exposure. Secondly, the coating promotes the formation of specific compounds on the surface of the sample, such as ZnO, which passivate the steel and reduce the active areas of the material. Coatings with higher thicknesses may

also have an impact on the structural stability due to the formation of microcracks and/or material detachments that could greatly affect the corrosion performance of the coating layer.

Despite the variations obtained in the electrochemical behavior of the three coatings immersed in simulated seawater at the different temperatures, after 7 days, the SEM/EDX analysis did not reveal any deterioration of the main coating layer. However, when observing the optical micrographs obtained after 30 days of exposure, it is possible to observe a red colored oxide on the surface, which is associated with the presence of iron oxides in the galvanized steel samples with lower thicknesses.

**Acknowledgements** I, A Sandoval-Amador, wish to extend my deepest gratitude to Natalia Gomez-Rios, my wife, for her unwavering support, boundless love, and remarkable patience throughout these years. Her encouragement has been the cornerstone of my journey, allowing me to navigate the challenges of scientific exploration with resilience and determination. Her belief in me has been an unyielding source of strength, shaping the very essence of this work. To her, I owe an immeasurable debt of gratitude for being my unwavering pillar of support, a beacon of love, and a source of endless patience. Thank you for being my rock through this scientific pursuit.

**Author contribution** JET-R: conceptualization, methodology, data collection, formal analysis, investigation, writing—original draft.

AS-A: conceptualization, methodology, validation, formal analysis, investigation, writing and editing

LFO-V: data curation, visualization, editing

DYP-B: validation, writing—review

JLE: writing—review and editing, supervision

All authors read and approved the final manuscript.



**Funding** The authors declare that no funds, grants, or other support were received during the preparation of this manuscript.

**Data availability** The raw data required to reproduce the above findings cannot be shared at this time due to time limitations; additionally, these data also form a part of an ongoing study.

## Declarations

**Conflict of interest** The authors declare no competing interests.

## References

- J.A. Ramírez-Jerez, M. Valero-Alvarado, D.Y. Peña-Ballesteros, J.E. Torres-Ramírez, *Rev. Fac. Ing* (2015). <https://doi.org/10.19053/01211129.3552>
- D.Y. Peña Ballesteros, A. Sandoval Amador, H.A. Estupiñán Durán, D. Sierra Fajardo, L. Quintero Ascanio, *Inf. Técnico*. (2015). <https://doi.org/10.23850/22565035.157>
- M.A. Azaroual, E.F. El Harrak, R. Touir, A. Rochdi, M.E. Touhami, *J. Mol. Liq.* (2016). <https://doi.org/10.1016/j.molliq.2016.04.117>
- A. Sandoval-Amador, J.E. Torres Ramirez, P.A. Cabrales-Villamizar, D. Laverde Cataño, D.Y. Peña-Ballesteros, *J. Phys. Conf. Ser.* (2017). <https://doi.org/10.1088/1742-6596/935/1/012052>
- C. Soriano, A. Alfantazi, *Constr. Build. Mater.* (2016). <https://doi.org/10.1016/j.conbuildmat.2015.11.009>
- P. Shreyas, B. Panda, A.D. Vishwanatha, *AIP Conference Proceedings*, vol 2317 (2021), p. 020038. <https://doi.org/10.1063/5.0036137>
- G.A. Gaber, L.Z. Mohamed, A. Abdelfatah, *Chem. Pap.* **77**, 7539–7549 (2023). <https://doi.org/10.1007/s11696-023-03043-4>
- R.S. Yeomans, in *Galvanized steel reinforcement in concrete*, ed. by R. ByS. Yeomans (Elsevier Science, 2004), p. 1. <https://doi.org/10.1016/B978-008044511-3/50016-5>
- L. Pugazhenthay, in *Indian metallurgy*, Indian Institute of Metals Series, ed. by R. By, S. V. S. N. Divakar, S. Murty, A. A. Srikanth, Gokhale. Galvanizing industry in India—Past, present & future (Springer, Singapore, 2024). [https://doi.org/10.1007/978-981-99-5060-7\\_13](https://doi.org/10.1007/978-981-99-5060-7_13)
- A.R. Marder, *Prog. Mater. Sci.* (2000). [https://doi.org/10.1016/S0079-6425\(98\)00006-1](https://doi.org/10.1016/S0079-6425(98)00006-1)
- S. Perme, L. Kingsley, *Constr. Build. Mater.* **392**, 131889 (2023). <https://doi.org/10.1016/j.conbuildmat.2023.131889>
- H. Sun, S. Liu, L. Sun, *Int. J. Electrochem. Sci.* **8**, 3494–3509 (2013). [https://doi.org/10.1016/S1452-3981\(23\)14407-5](https://doi.org/10.1016/S1452-3981(23)14407-5)
- X. Hou, L. Gao, Z. Cui, J. Yin, *IOP Conf. Ser. Earth Environ. Sci.* (2018). <https://doi.org/10.1088/1755-1315/108/2/022037>
- D. Thierry, D. Persson, N., in *Encyclopedia of interfacial chemistry*, ed. by W. Klaus. Le Bozec (Elsevier, Amsterdam, 2018), p. 55. <https://doi.org/10.1016/B978-0-12-409547-2.13431-6>
- G.A. El-Mahdy, A. Nishikata, T. Tsuru, *Corros. Sci.* (2000). [https://doi.org/10.1016/S0010-938X\(99\)00057-8](https://doi.org/10.1016/S0010-938X(99)00057-8)
- ASTM, E415-15 Standard test method for analysis of carbon and low alloy steel by spark atomic emission spectrometry. *ASTM Int.* (2017). <https://doi.org/10.1520/E0415-15>
- ASTM, A123/A123M-15 Standard specification for zinc (hot-dip galvanized) coatings on iron and steel products. *ASTM Int.* (2017). [https://doi.org/10.1520/A0123\\_A0123M-15](https://doi.org/10.1520/A0123_A0123M-15)
- ASTM, D1141-98, standard for the preparation of substitute ocean water. *ASTM Int.* **98** (1999). <https://doi.org/10.1520/D1141-98R13>
- ASTM G102, Standard practice for calculation of corrosion rates and related information from electrochemical measurements. *ASTM Int.* **89** (2016). <https://doi.org/10.1520/G0102-89R15E01.2>
- T. Bellezze, G. Giuliani, G. Roventi, *Corros. Sci.* (2018). <https://doi.org/10.1016/j.corsci.2017.10.012>
- V. Padilla, A. Alfantazi, *Corrosion* **69**(2), 174–185 (2013). <https://doi.org/10.5006/0645>
- S. Liu, H. Sun, L. Sun, H. Fan, *Corros. Sci.* (2012). <https://doi.org/10.1016/j.corsci.2012.08.056>
- M. Pourbaix, *Atlas of electrochemical equilibria in aqueous solutions* (Pergamon Press, London, 1966)
- F. Delaunoy, F. Tosar, V. Vitry, *Bioelectrochemistry*. (2014). <https://doi.org/10.1016/j.bioelechem.2014.01.003>
- V. Padilla, A. Alfantazi, *Constr. Build. Mater.* (2014). <https://doi.org/10.1016/j.conbuildmat.2014.05.053>
- M. Sabzi, S.M. Dezfuli, M. Asadian, A. Mahaab, *Mater. Res. Express* (2019). <https://doi.org/10.1088/2053-1591/ab10ad>

Springer Nature or its licensor (e.g. a society or other partner) holds exclusive rights to this article under a publishing agreement with the author(s) or other rightsholder(s); author self-archiving of the accepted manuscript version of this article is solely governed by the terms of such publishing agreement and applicable law.